

# Modelling and Extrapolation to Reactor Conditions

A. S. Kukushkin<sup>1</sup>, H. D. Pacher<sup>2</sup>

<sup>1</sup>ITER JCT, Boltzmannstr. 2, 85748 Garching, Germany

<sup>2</sup>INRS-Energie et Matériaux, Varennes, Québec, Canada

## Abstract

Recent results of divertor modelling at ITER JCT are summarised and a number of requirements to the code reflecting the reactor specifics are discussed. Some modelling results incorporated in the ITER divertor design, such as the beneficial effect of V-shaped targets, the importance of high gas conductivity between the divertors, and the role of deep core fuelling in maintaining the plasma density are discussed.

## 1. Introduction

Divertor modelling has become an essential tool for the design of the ITER divertor during the ITER EDA. Based on validation against present-day experiments, it allows the data from existing experiments to be extrapolated to the reactor conditions expected in ITER. The development of the codes has been continuing in parallel with the accumulation of experimental data, and the modelling results have strongly affected the evolution of the ITER divertor concept. The overall philosophy of the modelling studies for a reactor – i. e., for a machine which does not exist yet – is to use a code validated as well as possible against the present experiments, to use physically justified model assumptions and boundary conditions, and to check the results for trends which can be found in the present experiments. The paper describes the present status of reactor-oriented edge plasma modelling with a primary focus on its application to ITER.

Recent results of ITER divertor modelling have revealed several effects of the divertor geometry which can be verified against experimental data and are therefore taken into account in the divertor design. In particular, V-shaped targets facilitate the partial detachment of the divertor plasma near the separatrix strike points, reducing the peak power loads at given upstream density, and high gas conductance from the inner to the outer divertor is found to be important in enhancing radiation from the outer divertor, which has a higher power load. These issues, together with some other modelling results concerning ITER divertor performance and its compatibility with the core plasma are discussed in Section 2.

The quantitative difference in the main machine parameters between the reactor and present experiments changes the importance of several issues when reactor modelling is undertaken. High

output power causes a significant increase of the recycling particle fluxes, and long pulse duration leads to an equilibration of the particle content of the wall with the plasma, thereby leaving the particle balance to be sustained by pumping and fuelling – with fluxes two to three orders of magnitude lower than the recycling particle flux. This requires special attention to the quality of the particle balance in the code. A proper choice of the boundary conditions allows artefacts, such as unrealistic particle sources or impurity absorption in the plasma core, to be avoided, and is therefore crucial when extrapolative modelling is carried out. These issues are addressed in Section 3. Section 4 contains a discussion of several outstanding near-term problems in ITER edge modelling, and the conclusions are given in Section 5.

## 2. Recent results of ITER modelling

In this section, we summarise the results of application of the B2-Eirene code [1] to the analysis of the divertor for the latest modification of ITER (so called ITER-FEAT [2]). These studies have been undertaken since 1998 when the decision on the reduction of the machine cost, and hence the size, was taken [2]. The B2-Eirene code package realises a model consisting of a coupled 2D fluid model for the electrons and ions (B2) and a 2D Monte-Carlo model for atoms and molecules (Eirene). In most of the calculations quoted here, the plasma is assumed to consist of electrons and ions from D (representing both D and T), He, and C. All the ions have the same temperature  $T_i$ , which can be different from the electron temperature  $T_e$ , and each charge state is described as a separate fluid. Conventional sheath boundary conditions [1] are applied at the targets and a radial decay length of 3 cm is specified at the grid edges near the walls of the main chamber and in the private flux region (PFR). Finally, a uniformly distributed power flux carried by electrons and ions and either ion density or ion flux for each ion component are specified at the core-edge interface (CEI) – the innermost closed flux surface of the computation domain at the plasma core side. For the neutral particles, recycling conditions are applied on the targets and walls for gaseous species such as D and He, and full absorption is assumed for sticking species like C. The CEI is fully absorbing for neutrals, the pump duct entrance in PFR is modelled as a section of the wall with some absorption probability for incoming particles (several per cent, determined by the pumping speed), physical and chemical sputtering at the carbon-clad surfaces (targets and lower baffles) provide a self-consistent carbon source, and gas puffing is introduced from the top of the main chamber. At present, hydrocarbons are not considered, so that chemical sputtering immediately produces carbon atoms in the model.

The results are presented here in different cross-sections of a multi-dimensional operational window [3], mostly in the form of density scans. Indeed, the divertor must meet several constraints stemming from engineering limitations such as peak power load on the targets or particle throughput, on the one hand, and physical requirements of compatibility with the core plasma such as upstream

plasma density or helium concentration, on the other. Note that some of these limitations are not yet well defined and are the subject of ongoing studies and development.

## 2.1. Effect of the target shape

Design studies performed for ITER [3], mostly for a straight vertical target divertor geometry, have revealed that peak power loads are reduced when the targets meet the divertor bottom at an angle, forming a V-shape near the strike points, Fig. 1. The PFR side of the “V” helps to keep the neutrals in the vicinity of the strike point, thus favouring partial plasma detachment. The necessary depth of the “V” can be estimated from the requirement that the time it takes the plasma ions to reach the target from the opening of the “V” be comparable to the recombination time [4]. Our calculations show that partial detachment for ITER conditions occurs when the neutral density near the strike point is around  $10^{21} \text{ m}^{-3}$ , and the typical values of the plasma density and temperature there are  $10^{21} \text{ m}^{-3}$  and 1 eV, respectively. For such plasma parameters, the charge-exchange mean-free-path is around 1 mm, much less than the dimensions of this detachment (i.e., recombination) zone, and therefore the flux of neutrals leaving the recombination zone for the private flux region (PFR) where the pump duct is located, can be estimated using a diffusion approximation. The effective diffusivity for neutrals is

$$D \cong \frac{v_T^2}{v_{cx}} = \frac{v_T^2}{n \langle \sigma v \rangle_{cx}} \cong 10 \text{ m}^2 / \text{s},$$

where  $v_T$  is the thermal velocity of atoms and  $v_{cx}$  is the charge-exchange rate. For the conditions of the calculation with the "V", i.e. a typical cross-field distance of about 3 cm, a neutral density of  $10^{21} \text{ m}^{-3}$ , a major radius of the outer strike point  $R = 5.5 \text{ m}$ , and a flux to the pump (the particle throughput) of  $10^{23} \text{ s}^{-1}$  or less, one can estimate the poloidal length of the recombination zone in the absence of the “V” to be  $\sim 1 \text{ cm}$ . The neutral density in the PFR is around  $5 \cdot 10^{19} \text{ m}^{-3}$  (5 Pa at 1 eV), much lower than in the recombination zone. However, efficient recombination, given a recombination rate of  $\sim 10^4 \text{ s}^{-1}$  for these plasma parameters, a plasma fluid velocity  $\sim c_s \sim 10^4 \text{ m/s}$  and a pitch angle  $B_\theta/B_t \sim 0.1$ , would require a poloidal length of  $\sim 10 \text{ cm}$ , so that detachment would not yet occur in the absence of the "V".

If a V-shaped section of the divertor floor is introduced which has a wall 10 cm long, parallel to the separatrix and shielded by the “dome” (Fig. 1), the effect is indeed strong. Use of such a “V” reduces the peak power load by 30% compared with a straight vertical target for ITER-FEAT (see Fig. 2). This can outweigh the effect of the variation of the divertor length or the divertor closure. A reduction of the pumping speed causes a similar effect [3], i.e. increased neutral pressure in the divertor and reduced power load, but leads to a deterioration of helium removal – which is not the case for our modification of the target shape. Further optimisation of the divertor shape has resulted in the geometry shown in Fig. 3 (“new V”) which allows the power loading to be reduced further (“new V” points in Fig. 2). Note that the results for the “new V” in Fig. 2 are obtained with realistic gas

conductance between the divertors and the pump. This conductance takes the effect of the structures beneath the dome into account, and corresponds to a transparency lower by a factor 0.56 than that previously used (see next Section).

A similar trend was found in the JET experiments with strike point sweeping over the target corner [5]. It was shown that the V-shape of the target near the x-point facilitates partial detachment provided that the plasma density is sufficient to ensure neutral plugging.

## 2.2. Interplay of the inner and outer divertors

Most of the simple theoretical models used for qualitative analysis of divertor performance consider a single divertor with symmetry conditions upstream (see e. g. [6]). However, the presence of two divertors (inner and outer) with unequal power load introduces a new parameter which can be essential. Indeed, the natural asymmetry of the power loading between the inner and outer divertors causes a corresponding asymmetry of the plasma temperature near the target and this, given the balance of plasma pressure along the magnetic field, makes the recycling neutral flux in the inner divertor stronger than in the outer. As a result, a global particle circulation arises: the plasma flows along the magnetic field, mostly around the core, from the outer to the inner divertor, and this flow is balanced by a neutral flow from the inner to the outer divertor through the PFR. The gas conductance of the PFR becomes now an important parameter which controls the fuelling of the outer divertor by neutrals from the inner one.

In order to model this effect, two semi-transparent surfaces connecting the dome edges with the divertor bottom were introduced, Fig. 3 [4]. The transparency of these surfaces – that is, the probability  $\zeta$  that a particle impinging on the surface traverses it – was varied between 1 (surface fully transparent) and 0 (divertors closed to the PFR). The results are shown in Fig. 4 where the peak power load is plotted against the upstream density for different values of  $\zeta$ . The effect is clearly seen: reduction of the gas conductance between the divertors results on the whole in a considerable increase of the peak power loading (with saturation seen at  $\zeta = 0.25$  to 0.1). Comparison with a two-chamber model shows that the dome conductance prevails over the transparent wall conductance at  $\zeta > 0.5$ . The effective pumping speed  $S_p$  quoted in Fig. 4 is the ratio of the net particle outflow from both divertors toward the pump to the average pressure on the semi-transparent surfaces in Fig. 3.

The increase of peak power loading in the modelling is consistent with the JET experiments [7], where the introduction of a “septum” separating the inner and outer divertors was found to increase the asymmetry of the divertor parameters, i. e., the outer divertor became hotter and the inner one more detached. In that experiment, it was found that symmetry of the divertor parameters can be recovered by gas puffing in the outer divertor. This approach does not however look feasible in ITER:

the gas throughput between the divertors at  $\zeta = 1$  is calculated to be 300 to 400 Pa·m<sup>3</sup>/s, far beyond the pumping capability of ITER (DT throughput 100 to 200 Pa·m<sup>3</sup>/s). A sufficiently large gas conductance between the divertors in the PFR should therefore be provided in ITER, and the latest divertor design [8] corresponds to  $\zeta = 0.56$  (the value used for the “new V” results in Fig. 2).

### 2.3. Compatibility with the core plasma

The available experimental data in H-mode indicate that the separatrix density  $n_s$  is not expected to exceed 1/3 to 1/4 of the line average density [9]. This means that at least 2/3 or 3/4 of the core density must be built up in the “pedestal” region of the core plasma near the edge. The corresponding density gradient gives rise to an outward particle flux which has to be compensated by adequate fuelling inside the separatrix. Our studies [10] show that gas puffing in the main chamber, which is a technique commonly used in present-day experiments, would be quite inefficient in a reactor. In calculations for ITER with the gas puff from the top, the atomic DT flux across the separatrix increases but weakly with the puffing rate  $\Gamma_{DT\_puff}$ , staying almost constant for the high input power, Fig. 5. The scrape-off layer (SOL) plasma screens the core from both the puffed and the recycled neutrals. The gas puff is therefore a means of controlling the SOL and divertor density rather than the core density. Recent studies of core transport for ITER [11] have indicated the need to control the core fuelling intensity and profile. The present results together with those of [11] indicate that a significant part of this control will have to be performed via deep fuelling (e.g. pellets or low-energy beams).

Another way of rendering the core and edge densities consistent – an increase of  $n_s$  – may also be not so straightforward, even if it proves to be acceptable for the core confinement. Fig. 6 shows a variation of  $n_s$  with increase of the gas puffing rate [10]. The density increases and then saturates as  $\Gamma_{DT\_puff}$  is increased, accompanied by plasma detachment in the inner divertor. A further substantial increase of  $\Gamma_{DT\_puff}$  leads again to an increase of  $n_s$ , with the inner divertor now fully detached. The saturation level, both in  $n_s$  and throughput, increases with input power, and the rate of increase with  $\Gamma_{DT\_puff}$  of the recombination neutral source, and of the power radiated by neutrals increases where the density is saturated. This picture looks qualitatively similar to [6] where a theoretical model was developed which describes the saturation of  $n_s$  due to volume recombination. In that simplified model, only one divertor was considered, whereas in our case, it is the inner divertor, which carries the smaller part of the power and detaches first, that determines the saturation. A further density increase can occur once the detachment of the inner divertor is completed, and the outer divertor remains attached.

## 2.4. Effect of impurity seeding

Seeding the reactor plasma with a noble gas has been considered a possible means to enhance the radiation from the plasma edge and hence to reduce the target loading. Because this impurity seeding may become crucial if carbon has to be avoided as a plasma facing material because of high co-deposition of tritium [8], some modelling effort has been devoted to this problem [3, 4]. Assuming a constant impurity fraction in the plasma, one could expect that high-Z noble gases like Ar or Kr would be most efficient in terms of edge radiation power vs.  $Z_{eff}$  in the plasma because their radiation efficiency in the  $T_e$  range from 5 to 100 eV is much higher than that of C or Ne [9]. However, the results of B2-Eirene modelling show some qualitative difference from these simple estimates. First, if the edge power balance is dominated by carbon radiation, then additional neon seeding of the edge plasma mostly increases  $Z_{eff}$  with a minor effect on the radiated power [3]. In this case, neon simply replaces carbon as a radiator instead of adding to it. Indeed, the main carbon source in the model (and probably in reality) is chemical sputtering by hydrogen isotopes, which is largely proportional to the recycling particle flux. Once an extra radiating impurity is introduced into the plasma, the power remaining for hydrogen ionisation is lower, thus reducing the recycling flux and the carbon influx.

If a recycling impurity (Ar, Ne, or N) is introduced in a carbon-free divertor, then no strong difference between different impurity species is found [4]. The peak power loading on the target correlates mostly with  $n_s$  and  $Z_{eff}$  at the CEI, Fig. 7, so that no clear advantage of Ar over Ne is seen, and more detailed considerations on the spatial distribution of the impurities are required to elucidate the differences seen. Indeed, the reason for this unexpectedly weak dependence on the kind of the radiating impurity, in spite of the well-pronounced difference in the radiation efficiency [9], can be found in the impurity ion transport. Argon has higher radiation efficiency at low temperatures than neon, but the ionisation potentials of the same charge states for argon are lower. This means that for the same plasma temperature, argon ions are higher ionised and therefore subject to a stronger thermal force driving them upstream, towards higher temperatures where the radiation is less efficient – and where the  $Z_{eff}$  values are compared. Note that a similar effect, that is, a weak dependence of the radiated power on the impurity species used for discharge seeding, was reported from the JET experiment [12] – although the total radiation was considered there, not that from the edge.

## 2.5. Effect of helium atom scattering

Efficient helium removal is one of the most important functions of a divertor in a tokamak reactor. This efficiency is reflected by the helium concentration at the separatrix  $c_{He}$ , which must be kept low. The general picture of helium transport in the SOL and divertor can be described in the following way [13]. The helium ions leaving the core diffuse across the magnetic field to the outer, cooler part of the

SOL and flow to the targets there rather than in the hot part of the SOL adjacent to the separatrix, since in the latter region a thermal force drives them upstream in the direction of the temperature gradient, away from the target. After neutralisation at the outermost part of the target, the helium atoms have to cross the divertor plasma before they reach the pumping duct. Ionisation of helium atoms gives rise to helium recycling which increases  $c_{He}$ . Therefore plasma detachment, even partial, improves the helium removal efficiency by reducing helium recycling. For most of the ITER calculations performed so far, no collisions of helium atoms with the plasma ions were taken into account, and therefore helium atoms were not scattered in the plasma. Whereas such a neglect can be justified for charge-exchange collisions (low cross-section with ions of hydrogen isotopes and low concentration of helium ions), the elastic collisions with D (or T) ions can be important. These collisions both heat up the He atoms, thus increasing their mean-free-path, and scatter them in angle, increasing the probability of reaching the pumping duct. The overall result of including the elastic collisions of He atoms with background plasma ions is illustrated in Fig. 8. The effect on power loading is weak, because helium is not so important in the power balance. A significant (factor 3 to 5) reduction of  $c_{He}$  is observed, increasing with plasma density and giving a measure of a strong positive effect due to elastic collisions, which enhances the margins for divertor optimisation.

### 3. Reactor specifics in edge modelling

#### 3.1. Accuracy of particle balance

In a typical ITER case, because of high input power, the total neutral source due to plasma recycling and volumetric recombination is around  $10^{25} \text{ s}^{-1}$ , whereas the fuelling and pumping which are to be used to control the divertor operation amount to a particle throughput below  $10^{23} \text{ s}^{-1}$ . This means that the error in the particle balance in the model must be well below 1%, and this is a challenge for a hybrid code like B2-Eirene. The problem is that the ion transport is treated within the fluid model which is essentially implicit, whereas the neutral transport is modelled by a Monte-Carlo method and yields the particle sources for the fluid model, which are explicit. This leads to a violation of global particle balance during each time step for the fluid equations. Consider, for example, the particle balance during recycling on a single target. Let  $\Gamma_d$  be the ion flux to the target,  $\Gamma_p$  the neutral flux to the pump, and  $S$  the total ionisation source in the plasma. Then the neutral recycling flux  $I = \Gamma_d - \Gamma_p$  and the ion recycling flux  $S$  are equal after each call to Eirene, that is, before a B2 step, and they evolve differently during the B2 iterations. Indeed,  $\Gamma_d$  is the integral of the ion flow over the target, which depends on the local ion density, and  $S$  is an integral over the plasma volume of a source which has an implicit part (i.e. proportional to the ion density). The resulting discrepancy is normally within a few percent of the source, but this is still bigger than the pumped flux. In order to reduce this

discrepancy, scaling factors  $\alpha_i \approx 1$  can be introduced for each neutral source (denoted here by the subscript  $i$ ) with the values of  $\alpha_i$  adjusted in course of the B2 iterations so that the neutral and ion recycling fluxes remain in balance. Such a procedure, realised in the B2-Eirene code, allows improvement of the accuracy of the particle balance by 3 orders of magnitude, making it possible to study the effect of pumping and fuelling in ITER.

### 3.2. Boundary conditions at the core-edge interface

Since the plasma core is not included in the edge model, a proper set of boundary conditions should be selected at the CEI. The choice for the energy equations is rather obvious; we specify the power fluxes carried by electrons and ions. There are no significant energy sources in the edge, so that these fluxes set the scale for all energy source terms in the equations – and this makes a positive contribution to the numerical stability of the calculations. There is still some arbitrariness in the power split between the electrons and ions, but it does not lead to non-physical results.

Proper boundary conditions at the CEI for the continuity equations require more consideration. For interpretive modelling, the first choice would be specification of density. This quantity can be measured more easily than the particle flux, and such a boundary condition is convenient from the numerical standpoint. However, it may be not the best choice for extrapolative modelling. This density is not a well-controllable quantity and its use without other constraints, for example in density scans, may result in an unreasonably high particle flux from the core or in an unphysical particle flux into the core (we model a steady state, and there is no particle absorption in the core). The alternative boundary condition, specification of particle fluxes across the CEI, can only be applied meaningfully if the particle balance is improved as described above because these fluxes are usually very low compared to the recycling flux. The situation is more complicated for the impurities because of a possible interplay of different ionisation states in the core, and no accurate solution is available at the present time.

The results presented in Section 2 were obtained using various boundary conditions. For the straight target and “old V” configurations (2.1, 2.4), the  $D^+$  ion density at the CEI was specified and varied to make a density scan. The same was done for the gas conductivity study (2.2). The density scans with the “new V” geometry were done keeping the  $D^+$  ion flux across the CEI constant and varying the gas puffing rate. In all cases, the  $He^+$  density at the CEI was zero (justified by the plasma temperature of several hundred eV there) and the  $He^{++}$  density was adjusted to obtain the right balance between the source of helium (fusion power) and its flux to the pump. Since sputtering and absorption at the walls dominate the particle balance for carbon, zero particle fluxes across the CEI were specified for every charge state of C ions. Two different approaches were used for the seeded

impurities (2.4). One was to specify the density of the highest charge state and zero fluxes for the rest. This approximately corresponds to feeding impurities deep into the core and has been used for initial runs with Ne. The drawback of such a boundary condition is that the relative population of different charge states depends on the plasma temperature and that therefore a constant density of one particular charge state means variable particle influx. Another approach was to specify zero particle fluxes across the CEI and apply an impurity gas puff in the divertor. This was used for Ar, Ne, and N. In this case, the requirements to the impurity particle balance become more demanding.

#### **4. Discussion**

The introduction of V-shaped divertor targets described in Section 2.1 results in a trade-off between divertor performance and machine flexibility, which is very important for an experimental reactor like ITER. The primary problem here is the sensitivity of the divertor operation parameters (above all, power loading) to the strike point position, which can be controlled to a given but finite accuracy by the feedback control system. The first results on this sensitivity were reported in [10] where the  $q_{pk}$  variation with the plasma equilibrium modification due to the design values of the changes of the plasma current profiles was found to be acceptable. More work is needed to assess the effect of transient displacement of the strike points possible under feedback control of the plasma position.

The problem of good particle balance is more severe for impurities. Besides coupling with neutrals, a similar explicit-implicit approach is used in the code for the particle exchange between different charge states. This makes the computation more stable numerically, but at the expense of the accuracy of the particle balance. Furthermore, the concentration of seeded impurities is low, and this can compound the numerical difficulty. Work on this problem is under way, but reliable results are not available yet.

Elastic collisions with background plasma ions can be important also for neutral species other than helium atoms. For hydrogen atoms, they can hardly be distinguished from charge exchange which is included in the model. For the molecules, vibrational excitation should also be included. This process facilitates the break-up of molecules and thus counterbalances the effect of elastic collisions. For the carbon atoms, the scattering should be less important because of their higher ionisation rate, but it could play some role in the low-temperature region of partial detachment. In any case, these effects should be included in the model.

## **5. Conclusions**

Divertor modelling has made important contributions to the optimisation of the ITER divertor and this work is continuing. The recent divertor design accommodates several key points found in modelling and substantiated by existing experimental data, such as the beneficial effect of V-shaped divertor targets and the importance of high gas conductivity between the divertors in the private flux region. More attention is also being paid to deep fuelling methods such as pellet injection, which may be essential for core plasma fuelling given the recent modelling results on strong screening of the puffed neutrals by the SOL. More effort is required to clarify the potential of impurity seeding with different recycling gases. The first results indicate that there is less freedom of choice here than might have been expected, but the impurity transport model needs refinement before definite conclusions can be drawn. Recent modelling results obtained with elastic collisions of helium atoms with background plasma ions indicate that helium removal could be a less severe problem for ITER, and this observation expands the possibilities for divertor optimisation for reduction of the power loading.

Compared to interpretive modelling for the present-day experiments, reactor modelling has its own specific requirements and constraints. High recycling fluxes and long discharges increase the requirements on the accuracy of the particle balance in the code in order to be able to treat pumping and fuelling properly. Such an accuracy requires special efforts in the code.

## **Acknowledgement**

This report has been prepared as an account of work undertaken within the framework of the ITER EDA Agreement. The views and opinions expressed herein do not necessarily reflect those of the Parties to the ITER Agreement, the IAEA or any agency thereof. Dissemination of the information in this paper is governed by the applicable terms of the ITER EDA Agreement.

## References

- [1] D. Reiter, H. Kever, G.H. Wolf, et al., *Plasma Phys. and Contr. Fusion*, **33** (1991) 1579; R. Schneider, D. Reiter, H.-P. Zehrfeld, et al. *J. Nucl. Mater.*, **196–198** (1992) 810.
- [2] G. Janeschitz, ITER JCT and HTs, *J. Nucl. Mater.*, **290–293** (2001) 1
- [3] A. S. Kukushkin, G. Janeschitz, A. Loarte, et al., *J. Nucl. Mater.*, **290–293** (2001) 887.
- [4] A. S. Kukushkin, H. D. Pacher, G. Janeschitz, et al., to appear in *Nucl. Fusion* (2001)
- [5] A. Loarte, *Nucl. Fusion* **38** (1998) 587; R. Monk, A. Loarte, S. J. Davies, et al., Proc. 24<sup>th</sup> EPS Conf. Contr. Fusion Plasma Phys., Berchtesgaden, 1997, ECA Vol. 21A, p. 117.
- [6] S. I. Krasheninnikov, M. Rensink, T. Rognlien, et al., *J. Nucl. Mater.* **266–269** (1999) 251.
- [7] C. F. Maggi, G. D. Conway, G. Corrigan, et al., Proc. 26<sup>th</sup> EPS Conf. on Contr. Fusion and Plasma Phys., Maastricht, 1999, ECA Vol. 23J (1999) 201.
- [8] G. Janeschitz, et al., “Divertor Design and Its Integration into the ITER Machine”, Proc. 18<sup>th</sup> Fusion Energy Conference, Sorrento, 2000.
- [9] ITER Physics Basis. *Nucl. Fusion* 39 (1999) 2137.
- [10] A. S. Kukushkin, H. D. Pacher, G. Janeschitz, et al., “Operational Space of a Shaped Divertor in ITER”, Proc. 28<sup>th</sup> EPS Conf. on Contr. Fusion and Plasma Phys., Funchal, 2001.
- [11] G. W. Pacher, H. D. Pacher, G. Janeschitz, et al., "H-mode Operation in ITER: Determination of Trajectories in Edge Operational Space", Proc. 28<sup>th</sup> EPS Conf. on Contr. Fusion and Plasma Phys., Funchal, 2001.
- [12] G. F. Matthews, B. Balet, J. G. Cordey, et al., *Nucl. Fusion*, **39** (1999) 19.
- [13] S. I. Krasheninnikov, A. S. Kukushkin, T. K. Soboleva, *Nucl. Fusion*, **31** (1991) 1455.

## Figure captions

Fig. 1. Variation of the divertor geometry used to study the effect of the “V” (straight vs. “old V”).

Fig. 2. Variation of the peak power loading of the target for three values of the power entering the SOL. Circles correspond to the “old V” geometry in Fig. 1, squares and triangles to the “new V” geometry shown in Fig. 3.

Fig. 3. Model geometry used for the gas conductance study (“new V”). Thick dashed lines show the semi-transparent liner surfaces and arrows indicate a typical neutral flow pattern.

Fig. 4. Peak power vs. upstream density for V-shaped target. Input power 100 MW, varying effective pumping speed  $S_p$  ( $\text{m}^3/\text{s}$ ) is shown for comparison.  $\zeta$  is the probability that a neutral particle impinging on the liner under the dome traverses it.

Fig. 5. DT atom influx into the core vs. gas puffing rate for the divertor geometry shown in Fig. 3. For notations, see the legend in Fig. 2.

Fig. 6. Upstream plasma density vs. DT particle throughput for  $S_p = 20 \text{ m}^3/\text{s}$  and different values of the input power.

Fig. 7. Divertor performance with impurity seeding: peak power loading vs. upstream plasma density (a) and  $Z_{\text{eff}}$  at the CEI vs. DT particle throughput (b). The curve corresponding to the intrinsic carbon impurity as the radiator is also shown for comparison. The input power is 86 MW, effective pumping speed  $75 \text{ m}^3/\text{s}$ , straight target.

Fig. 8. Effect of He atom scattering: peak power loading on the target  $q_{pk}$  vs. upstream plasma density  $n_s$  (a) and relative helium concentration at the separatrix  $c_{He}$  vs. DT particle throughput  $\Gamma_{DT}$  (b) for different values of the input power. Cases with 100 and 130 MW have the same fusion power of 600 MW and helium production rate, cases with 86 MW have fusion power and helium production rate lower by factor 1.5.

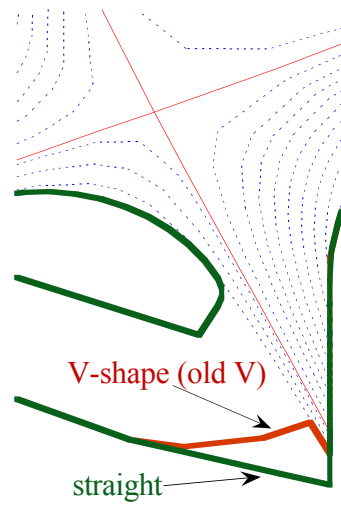


Fig. 1

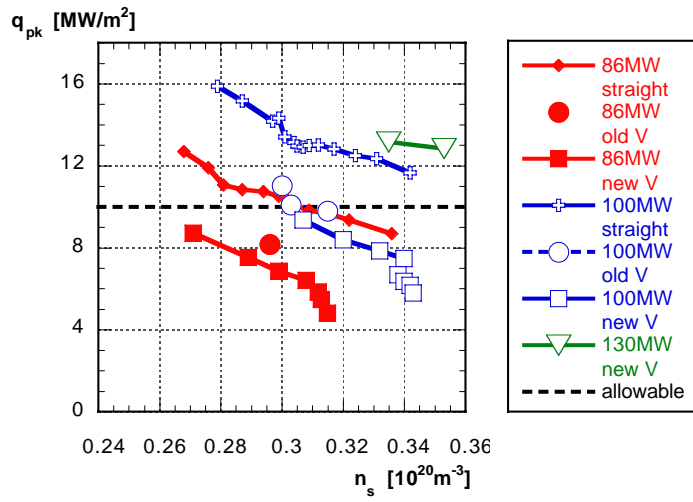


Fig. 2

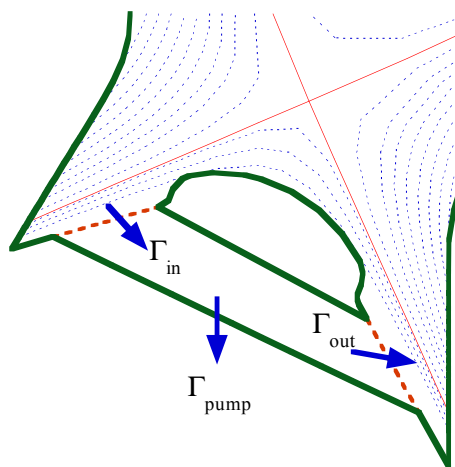


Fig. 3

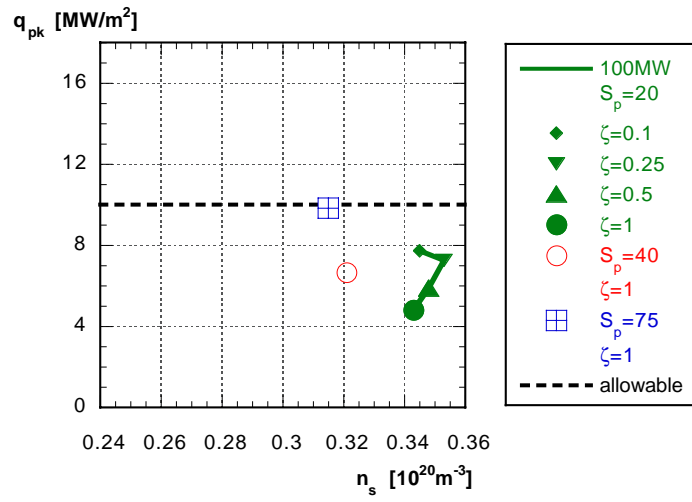


Fig. 4

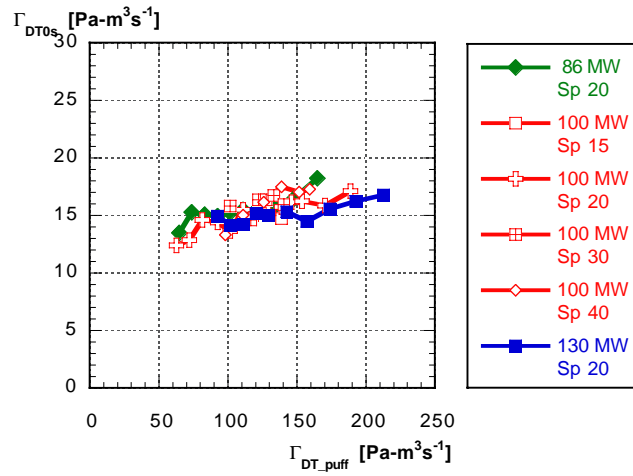


Fig. 5

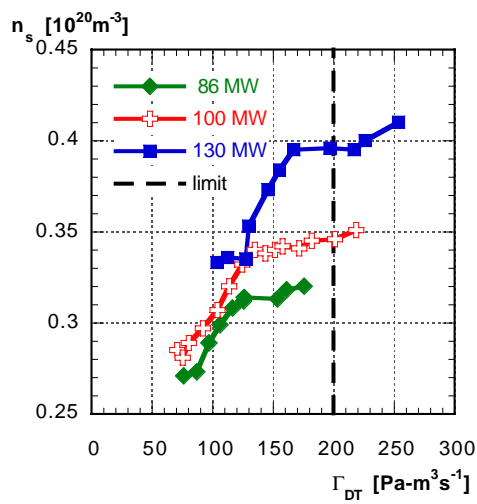
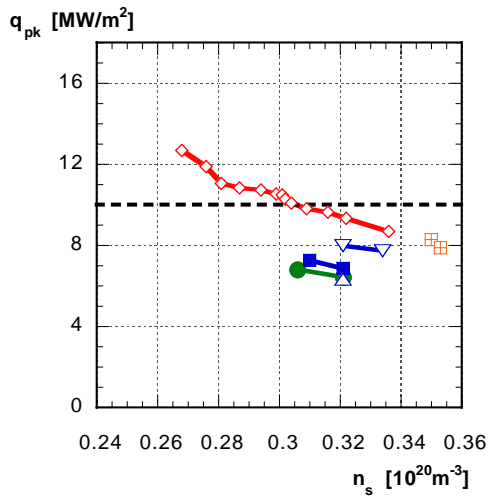
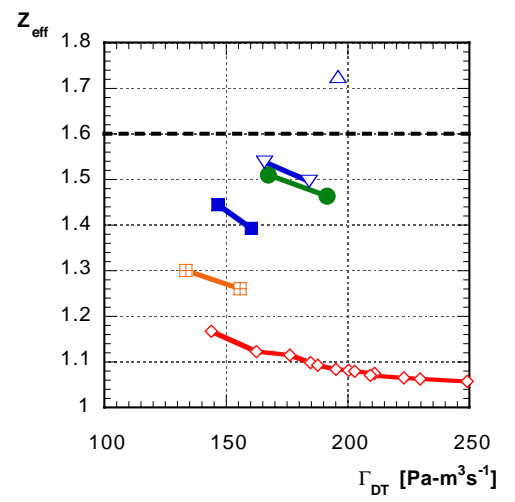


Fig. 6

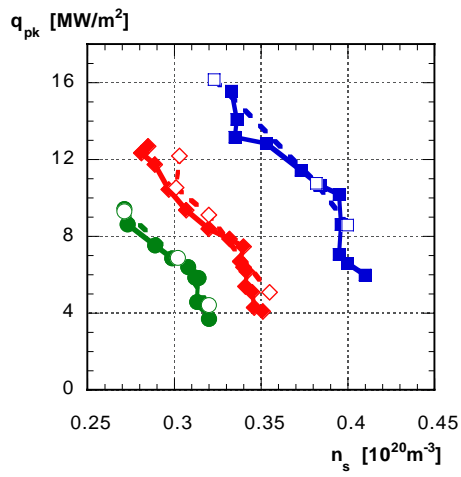


(a)

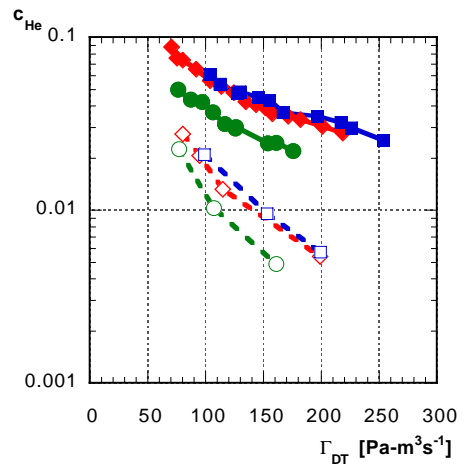


(b)

Fig. 7



(a)



(b)

Fig. 8